

# Reference-Based 3D-Aware Image Editing with Triplane

Bahri Batuhan Bilecen<sup>1</sup>, Yigit Yalin<sup>1</sup>, Ning Yu<sup>2</sup>, and Aysegül Dundar<sup>1</sup>

<sup>1</sup> Bilkent University, Computer Science Department

<sup>2</sup> Netflix Eyeline Studios

**Abstract.** Generative Adversarial Networks (GANs) have emerged as powerful tools not only for high-quality image generation but also for real image editing through manipulation of their interpretable latent spaces. Recent advancements in GANs include the development of 3D-aware models such as EG3D, characterized by efficient triplane-based architectures enabling the reconstruction of 3D geometry from single images. However, scant attention has been devoted to providing an integrated framework for high-quality reference-based 3D-aware image editing within this domain. This study addresses this gap by exploring and demonstrating the effectiveness of EG3D’s triplane space for achieving advanced reference-based edits, presenting a unique perspective on 3D-aware image editing through our novel pipeline. Our approach integrates the encoding of triplane features, spatial disentanglement and automatic localization of features in the triplane domain, and fusion learning for desired image editing. Moreover, our framework demonstrates versatility across domains, extending its effectiveness to animal face edits and partial stylization of cartoon portraits. The method shows significant improvements over relevant 3D-aware latent editing and 2D reference-based editing methods, both qualitatively and quantitatively. Project page: [three-bee.github.io/triplane\\_edit/](https://three-bee.github.io/triplane_edit/)

**Keywords:** 3D-aware editing · Reference-based editing · EG3D

## 1 Introduction

In recent years, the high-fidelity image synthesis performance has been profoundly transformed by the emergence of Generative Adversarial Networks (GANs) [12, 18, 19]. Through adversarial training, they learn to map random distributions to actual data observations, thereby enabling the generation of photo-realistic images from latent codes. The evolution of GANs from 2D into 3D-aware [5, 6, 13, 28] has further boosted this capability, integrating hybrid 3D representations and Neural Radiance Fields (NeRF) [27] into style-based generators, yielding unparalleled success in crafting highly realistic 3D portraits.

The application of GANs extends beyond generation, venturing into real image editing through GAN inversion [3, 31, 35, 40, 42] and manipulation of the latent space [33]. A critical challenge in reference-based image editing via this

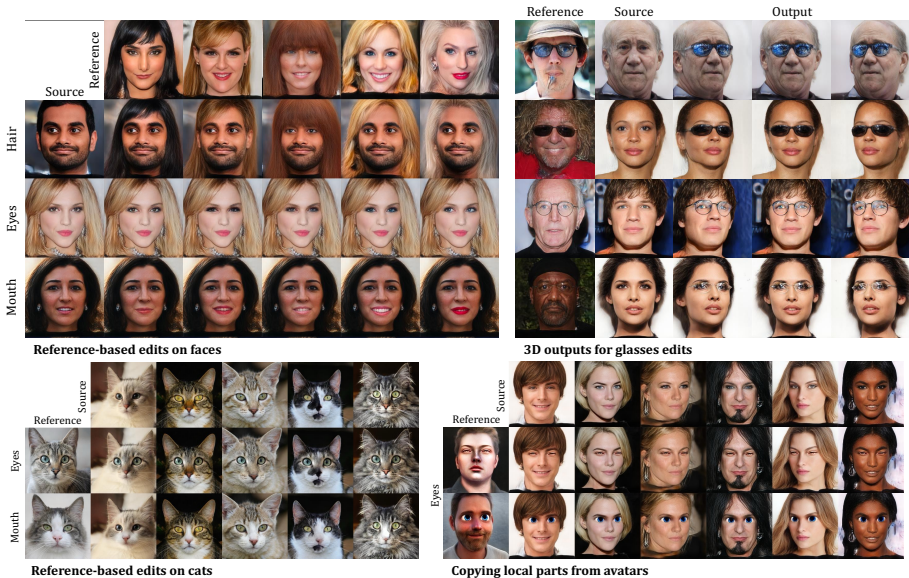


**Fig. 1:** Our approach excels in reference-based edits, faithfully reproducing the copied reference parts. Leveraging 3D-aware triplanes, our edits are versatile, allowing for rendering from various viewpoints. Additionally, we demonstrate successful edits on animal faces and even replicate references from cartoon portrait faces.

latent space is striking the optimal balance between retaining essential elements from the input image and incorporating desired attributes from the reference image. This balance is crucial to avoid overshadowing the input image’s essence in the editing process, thereby maintaining its identity while still leveraging the reference’s attributes. This dilemma presents itself as a complex problem of disentanglement and fusion, requiring the identification and integration of relevant feature components from both the reference and input images within the latent space to produce the desired edited output.

Despite the advancements in this domain, there is a noticeable gap in the development of reference-based, 3D-aware image editing techniques. Existing methods in 3D-aware image editing lack reference-based capabilities [20,42], while current reference-based editing approaches do not support 3D-awareness [8,21] or facilitate local editing [29,33]. Addressing this gap, our work focuses on pioneering reference-based, 3D-aware image editing, where we learn spatial disentanglement and fusion within the triplane latent space of the EG3D generator [5]. Our primary motivation stems from the fact that triplanes can be manipulated for editing purposes akin to the 2D image domain but offer distinct advantages. Triplanes not only facilitate 3D editing but also alleviate alignment issues inherent in 2D image space. For example, transferring an eyeglass from one person to another in 2D necessitates precise alignment in the image space. Conversely, in the triplane space, stitching is facilitated as images with varying camera parameters

can be rendered from the canonical triplane space. However, ensuring seamless boundaries requires additional steps. To accomplish reference-based image editing through triplane feature manipulations, our framework localizes parts within the triplane space and then fuses them using the encoders that we train.

Our contributions span the following thrusts:

1. We are at the forefront of conceptualizing reference-based 3D-aware image editing as an integrated framework. Our approach includes encoding triplane features, spatial disentanglement with automatic localization of features, and fusion learning for desired image editing. Our framework offers a novel perspective on how to tackle 3D-aware image editing by leveraging reference images.
2. Our work establishes new benchmarks for both quantitative and qualitative assessment in the field of reference-based image editing. Our framework demonstrates superior performance, surpassing four of the most recent baseline methods in 3D-aware latent editing and 2D reference-based editing applications. This advancement is quantified by significant improvements in FID metric for quality and pixel-wise metrics for source preservation.
3. We extend the effectiveness of our framework towards cartoon portraits and animal faces, showcasing its versatility and generalizability across different domains as shown in Fig. 1. This extension not only broadens the applicability of our approach but also underlines its potential in diverse and creative image editing contexts.

## 2 Related Works

**StyleGAN inversion-based editing.** It has been shown that well-trained GAN models organize their latent space in a semantically meaningful way that enables edits via vector arithmetic in the latent space. Especially for StyleGAN models [19], many methods are proposed to find interpretable directions in unsupervised ways such as GANSpace [14], StyleFlow [2], StyleSpace [36], StyleCLIP [29] and supervised ways such as InterFaceGAN [33]. These methods are combined with real image inversion methods so that an image is projected onto StyleGAN’s latent space and is edited [30, 31]. Recently, EG3D [5] augmented StyleGAN architecture with a triplane that provides efficient 3D-aware representation and a differentiable rendering mechanism to extend 2D image generation capabilities to 3D-aware generations. For this new domain, new image inversion methods are proposed [38, 41, 42]; however, for editings, previous methods such as InterFaceGAN and StyleCLIP are re-used. In this work, we explore a new editing domain for EG3D, namely triplanes, which encode canonical information of image models. We take advantage of the canonical representations which allow us to copy-paste features between triplane representations because of their alignment. Our method achieves reference-based editing which was not possible with previous StyleGAN editing methods.

**Reference-based image-to-image translation.** We refer to the models that are end-to-end trained for editing applications as image-to-image translation

methods. They are different than StyleGAN inversion-based edits because StyleGAN is not trained for image translation tasks yet achieves that by its interpretable latent codes. On the other hand, image-to-image translation methods are trained to change selected attributes of images while preserving the content [7, 11, 16, 21, 22, 26, 32, 37, 43]. This is usually achieved by an encoder-decoder architecture. Specifically, they include an encoder for the reference image and another encoder or shared one for the source image [7, 17, 21, 25, 39, 46, 47]. After the encodings and manipulations in encoded latent spaces, the translated image is generated via the decoder. In these models, the reference style can be sampled from a normal distribution followed by mapping functions or it can be encoded from a reference image [8, 9, 21]. One major limitation of these works is that they require labeled datasets for each attribute, and models such as VecGAN [9] and HisD [21] can only achieve a handful of edits such as change in hair color, smile, gender, eyeglasses, age, and adding and removing bangs by using the labels of CelebA dataset [24]. Because they rely on labeled data, those works are mostly developed for human face editing tasks; whereas we show edits of both portraits and animals. They also work on 2D images and are not able to provide a multi-view consistent 3D representation. Our method achieves editing on 3D triplane space and outputs an edited 3D model. In addition, unlike previous reference-based methods, our approach can achieve local edits, such as copying features like the mouth and nose from a reference image. This capability distinguishes it from traditional reference-based translation methods, which primarily focus on learning attribute changes, such as making someone appear older or younger. Such methods accomplish this by training models on separate sets of images: one featuring younger individuals, and the other one featuring elders.

### 3 Method

This section explains the details of our three-stage triplane editing pipeline. Our main motivation lies within the fact that triplanes can also be stitched and blended for editing just like in the 2D image domain, but it has advantages over the 2D domain. Triplanes not only yield 3D editing results but also eliminate alignment challenges present in the 2D image space. For instance, copying eyeglasses from one person to another in 2D requires alignment in the image space. In contrast, triplane space allows for straightforward stitching as images with different camera parameters can be rendered from the same canonical triplane space. However, achieving seamless boundaries requires additional steps.

#### 3.1 Localizing parts in the triplane space

The most direct way to perform a region transfer from reference to source image would be to mask the region of interest accordingly and apply blending. However, this process becomes intricate in hybrid 3D representations like triplanes due to the absence of a conventional method for identifying the regions to be masked.

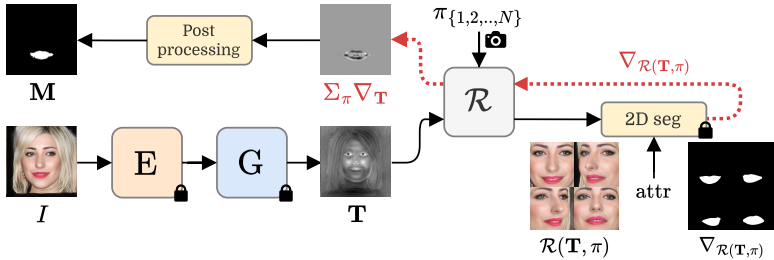


**Fig. 2:** Triplane part localization stage, where  $E$ ,  $G$ , and  $\mathcal{R}$  are encoder [4, 42], generator [5], and neural volumetric renderer, respectively. For the 2D segmentation model, we use state-of-the-art off-the-shelf segmentation models [1]. Images other than the input image are cropped to zoom in for visualization purposes. The pipeline does not have any cropping.

To address this, we take advantage of the volumetric renderer used in [5] being fully differentiable, and back-propagate the 2D image domain masks to the 3D hybrid triplane domain to create triplane masks (Fig. 2). More specifically, we first encode the input images via a pre-trained model [4, 42] to output triplane features. Next, we render the triplane  $\mathbf{T}$  with various camera poses  $\pi_{1,2,\dots,N}$  to obtain a collection of multi-view 2D renderings  $\mathcal{R}(\mathbf{T}, \pi)$  of the subject  $\mathbf{T}$ , and employ an off-the-shelf face segmentation network on the image domain to find the masks for the face attributes of interest (such as hair, eyes, glasses, etc.) for each rendering. We assign each masked rendering as the output gradient  $\nabla_{\mathcal{R}(\mathbf{T}, \pi)}$ , and find the input gradient  $\nabla_{\mathbf{T}}$  via autograd through the renderer  $\mathcal{R}$ . This process is iterated for  $N$  multi-view renderings, allowing us to accumulate the input gradients  $\Sigma_{\pi} \nabla_{\mathbf{T}}$  and localize the triplane mask.

While using the gradient mask alone may yield sub-optimal results, obtaining a valid mask  $\mathbf{M}$  only requires minor adjustments. The range of  $\Sigma_{\pi} \nabla_{\mathbf{T}}$  is not suitable for masking (not between 0-1), and the valuable information is accumulated around the mean value of each channel. Hence, as the post-processing step, we only keep a close neighborhood around the mean determined by  $\epsilon$  for each 96 channel (the channel size of the triplane), perform channel-wise min-max normalization, and apply binary thresholding with threshold  $\gamma$ . The parameters  $\epsilon, \gamma$  are provided in the Supplementary. These parameters are set once and used across all experiments for each attribute and domain. This localization is done both for source and reference images.

For scenarios such as glasses, where finer granularity in the triplane mask is required as we do not want to copy the eyes but only the glasses and the frame, we can employ common  $W^+$  directions explored by methods such as InterfaceGAN [33]. More clearly,  $w$  being the latent code of the corresponding sample with eyeglasses, and  $w_{\text{attr}}$  the direction towards the attribute, we construct  $\Delta \mathbf{T}_{\text{attr}} = G(w) - G(w - w_{\text{attr}})$ . Here,  $G(w - w_{\text{attr}})$  corresponds to the

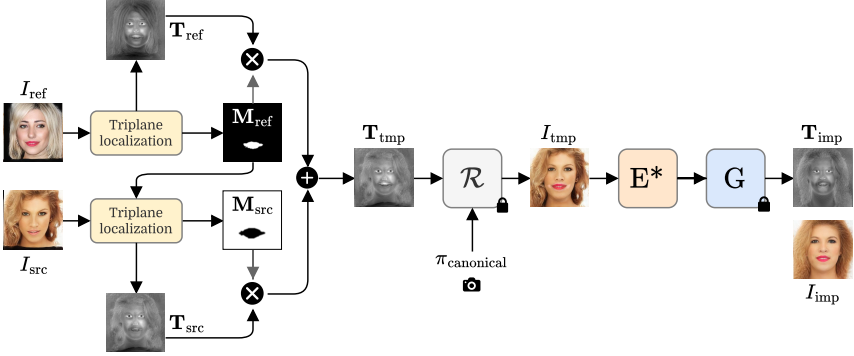


**Fig. 3:** Triplane localization and implicit fusion stages, where  $E^*$  denotes the fine-tuned image encoder that is described in Sec. 3.3. Straightforward stitching in the triplane results in color inconsistency across the boundaries as shown in  $I_{tmp}$  (zoom in for details). Leveraging  $E^*$ , we aim to attain seamless boundaries and produce outputs with a natural appearance.

triplane with eyeglasses removed. We multiply the output triplane mask with post-processed  $\Delta \mathbf{T}_{attr}$  to aid better localization of the selected attribute.

### 3.2 Implicit fusion by encoding & decoding

After finding suitable masks for reference and destination triplanes,  $\mathbf{M}_{ref}$  and  $\mathbf{M}_{src}$  respectively, a naive approach would be to follow Eq. (1):

$$\mathbf{T}_{tmp} = \mathbf{M}_{ref} * \mathbf{T}_{ref} + \mathbf{M}_{src} * \mathbf{T}_{src} \quad (1)$$

However, Fig. 6 (V1) reveals only using Eq. (1) distorts the geometry and color consistency, and creates stitching seams around the editing borders. In addition, in some cases, the contents in  $\mathbf{T}_{ref}$  and  $\mathbf{T}_{src}$  are not enough to ensure the editing looks natural around the region where two masks meet, necessitating the hallucination of additional content to complement the editing. For example, we may want to remove the long hair from the source image and replace it with the short hair from the reference image. In this case, the pixels that correspond to long hair regions need to be filled similar to an inpainting task.

Given the above observations and because GANs latent spaces embed natural images, we render the naively fused triplane with the canonical pose, re-encode it via the image encoder  $E_{W^+}$ , and re-decode via the generator  $G$  to obtain an implicitly fused triplane, shown in Eq. (2):

$$\mathbf{T}_{imp} = G(E_{W^+}(\mathcal{R}(\mathbf{T}_{tmp}, \pi_{can}))) \quad (2)$$

Note that state-of-the-art image inversion methods for EG3D, such as GOAE [42] and TriPlaneNet [4], employ both low-rate  $W^+$  and high-rate  $F^+$  codes. The latter is crucial for reconstructing fine image details. However, our objective in

this phase is not to achieve perfect image reconstruction. On the contrary, we aim for the encoder to map the image to a latent space with realistic reconstructions. To achieve this, we disable the high-frequency restoration branch of  $E_{W^+}$  at this stage to prevent encoding visible seams. This allows us to project the edited image onto its nearest natural representation on  $G$ 's manifold, implicitly fusing the masked triplanes. The output of this step can be seen in Fig. 3 showcasing seamless boundaries across the stitches. However, image details are also compromised at this stage, as we solely depend on the encoded low-rate  $W^+$  space, which is constrained in its expressive power due to the information bottleneck.

To bring the image details back, we employ  $\mathbf{T}_{\text{imp}}$  at the transition regions, as depicted in Eq. (3). For example, when we transfer the mouth from a reference image to our source image, we aim for the triplane features outside the mouth to originate from the source  $\mathbf{T}_{\text{src}}$ , the mouth features from the reference,  $\mathbf{T}_{\text{ref}}$ , and features across the boundaries from  $\mathbf{T}_{\text{imp}}$ .

$$\mathbf{T}_f = \mathcal{E}(\mathbf{M}_{\text{ref}}) * \mathbf{T}_{\text{ref}} + \mathcal{E}(\mathbf{M}_{\text{src}}) * \mathbf{T}_{\text{src}} + (\mathcal{E}(\mathbf{M}_{\text{src}}) - \mathcal{E}(\mathbf{M}_{\text{ref}})) * \mathbf{T}_{\text{imp}} \quad (3)$$

Here,  $\mathcal{E}$  denotes morphological erosion. We also apply Gaussian blurring with parameters  $(\mu, \sigma)$  onto the masks to avoid sharp edges and tune the kernel sizes for  $\mathcal{E}$ 's alongside with  $(\mu, \sigma)$ . The hyperparameters are provided in the Supplementary. This step is not illustrated in Fig. 3 for brevity.

Finally,  $\mathbf{T}_f$  is rendered from any desired pose  $\pi_R$ , and the final image is obtained, as illustrated in Eq. (4).

$$I_{\text{edited}} = \mathcal{R}(\mathbf{T}_f, \pi_R) \quad (4)$$

### 3.3 Fine-tuning the image encoder

Although  $\mathbf{T}_{\text{imp}}$  obtained in Sec. 3.2 helps tremendously even though a pre-trained encoder is used to obtain it, we notice in some cases where we have skin color inconsistencies, background leakages, and missing high-frequency details around the editing regions (Fig. 6 (V2)). Hence, we fine-tune implicit fusion image encoder  $E_{W^+}$  jointly with the triplane editing pipeline to mitigate the aforementioned effects.

During the fine-tuning phase, we employ masked losses to guide  $E_{W^+}$  in encoding only the visible regions, as illustrated in Fig. 4. To ensure that reconstruction losses do not affect the boundaries, we dilate the masks estimated by 2D segmentation models.

We generate renders for various viewpoints from both the source and reference images corresponding to different attributes. Once masked, these renders serve as ground-truths for our model. For instance, as shown in Fig. 4, if our objective is to transfer the hair from the reference image, we mask out the reference renderings to exclude pixels that do not represent hair, while doing the opposite for the source ground truths. After they are masked, they provide us

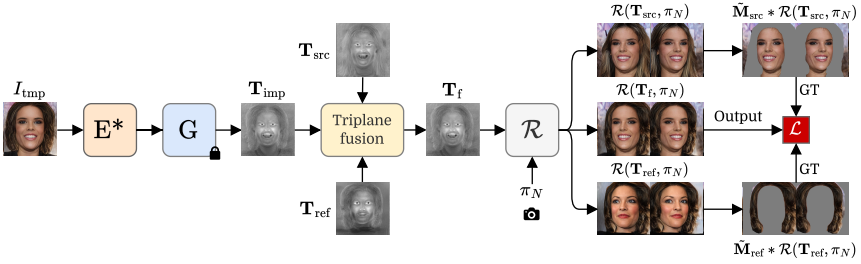


**Fig. 4:** Pipeline for the implicit fusion encoder fine-tuning. We generate masked ground truths for our task by utilizing 2D segmentation networks and via renderings from multiple views. Our goal is to carry the reference parts in great detail to our source image while preserving the identity of the source. Triplane fusion corresponds to Eq. (3).

with the ground-truths. The output of our model  $\mathbf{T}_f$  is obtained by the fusion process given in Eq. (3).

The objective to be minimized is provided in Eq. (5):

$$\min_E \lambda_{\mathcal{F}} \mathcal{L}_{\mathcal{F}}(\mathcal{D}(\tilde{\mathbf{M}}_{\text{ref}}) * \mathcal{R}(\mathbf{T}_f, \pi_N), \mathcal{D}(\tilde{\mathbf{M}}_{\text{ref}}) * \mathcal{R}(\mathbf{T}_{\text{ref}}, \pi_N)) + \lambda_{\text{ID}} \mathcal{L}_{\text{ID}}(\mathcal{D}(\tilde{\mathbf{M}}_{\text{src}}) * \mathcal{R}(\mathbf{T}_f, \pi_N), \mathcal{D}(\tilde{\mathbf{M}}_{\text{src}}) * \mathcal{R}(\mathbf{T}_{\text{src}}, \pi_N)) \quad (5)$$

where  $\mathcal{L}_{\mathcal{F}}$  is the learned perceptual image patch similarity loss (LPIPS) [45],  $\mathcal{L}_{\text{ID}}$  is the identity similarity loss [10],  $\mathcal{D}$  is dilation operation, and  $\tilde{\mathbf{M}}_{\text{src}}$  and  $\tilde{\mathbf{M}}_{\text{ref}}$  are the corresponding 2D segmentation masks for the rendered images  $\mathcal{R}(\mathbf{T}_{\text{src}}, \pi_N)$  and  $\mathcal{R}(\mathbf{T}_{\text{ref}}, \pi_N)$  with poses  $\pi_N$ , respectively.

To achieve identity preservation of the source image, we rely on the ID losses, and to copy the attribute with details, we rely on the LPIPS score from Eq. (5). We omit pixel-wise losses like  $\mathcal{L}_{L_2}$  since they are highly dependent on the quality of the off-the-shelf 2D segmentation network. During the fine-tuning, we use each subject tuple  $(\mathbf{T}_{\text{src}}, \mathbf{T}_{\text{ref}})$  multiple times, rendered from randomly chosen  $\pi$ 's.

Compliant with the common encoder training methodology, we use FFHQ [18] and AFHQ [7] as our training sets for our face and cat experiments, respectively. We employ Ranger optimizer, which is a combination of Rectified Adam [23] with Lookahead [44]. The learning rate is set to  $1e^{-4}$ , and fine-tuning is done for 1500 steps with a batch size of 2 on a single GPU.

## 4 Experiments

**Evaluation.** We present metrics evaluating both the reconstruction and editing qualities of our approach. For editing assessment, we employ the Fréchet Inception Distance (FID) metric [15], which evaluates realism by comparing the distribution of target images with that of edited images. Specifically, we compute

**Table 1:** Quantitative scores for various edits on CelebA.

	Eyeglasses			Hair		
	FID ↓	$\mathcal{M}_{\text{SSIM}} \uparrow$	$\mathcal{M}_{\mathcal{L}_2} \downarrow$	FID ↓	$\mathcal{M}_{\text{SSIM}} \uparrow$	$\mathcal{M}_{\mathcal{L}_2} \downarrow$
HiSD [21]	77.56	0.9471	0.0090	94.53	<b>0.9743</b>	0.0036
VecGAN++ [8]	71.47	0.7483	0.0630	80.47	0.9296	0.0090
InterfaceGAN [33]	88.13	0.9398	0.0104	80.93	0.7888	0.0387
StyleCLIP [29]	80.13	0.8421	0.0476	92.60	0.8716	0.0196
<b>Ours</b>	<b>66.68</b>	<b>0.9818</b>	<b>0.0021</b>	<b>64.59</b>	0.9720	<b>0.0029</b>

FIDs for the addition of eyeglasses and hair edits from black to blonde transition, where we use the CelebA dataset. By leveraging ground-truth attribute labels, we add eyeglasses to images that do not have eyeglasses and compute FIDs between the resulting edited images and original images that already have eyeglasses. This process is repeated for hair edit as well.

For reconstruction, we mask the edited areas and find pixel differences between the input and edited images. For example, for the eyeglasses edit, we mask out the eyeglasses and find the L2 distance and SSIM for the unmasked pixels.

**Baselines.** We conduct comprehensive comparisons by evaluating our editing methods against both reference-based 2D image editing methods and StyleGAN-based editing methods. Note that there are no reference-based editing methods that achieve 3D reconstruction under one framework. The reference-based 2D image editing methods, HiSD and VecGAN++, via end-to-end image translation networks output 2D images. On the other hand, InterfaceGAN and StyleCLIP are proposed for finding editing directions in  $W^+$  space for StyleGAN and have also been shown to work on 3D-aware GAN methods. They cannot achieve reference-based image editing but can change different attributes of images.

**Results.** We present both quantitative and qualitative comparisons with competing methods in Tab. 1 and Fig. 5, respectively. From Tab. 1, it’s evident that our method outperforms competing methods significantly in terms of FID and preserves pixels better in the non-edited regions. In Fig. 5, our method successfully adds eyeglasses to source images with remarkable fidelity to the reference image. In contrast, HiSD and VecGAN++ encounter difficulties in achieving fidelity to the reference image eyeglasses, likely due to their encoding of images into low-rate latent spaces for feature extraction. Operating in a higher-dimension triplane space allows us to overcome this limitation. Additionally, the canonical nature of the triplane ensures that even with variations in facial pose, the eyeglass region remains consistent which poses a challenge for 2D image methods. In both the InterFaceGAN and StyleCLIP methods, users lack control over the appearance of the added eyeglasses. Notably, these methods consistently produce similar-looking eyeglasses when applied to different inputs.

When discussing hair edits, it is essential to highlight that our method transfers the hair from the reference image to our inputs, whereas other methods only alter the hair color. In our quantitative analysis, we ensure fairness by masking the unedited areas based on hair predictions from the segmentation network.

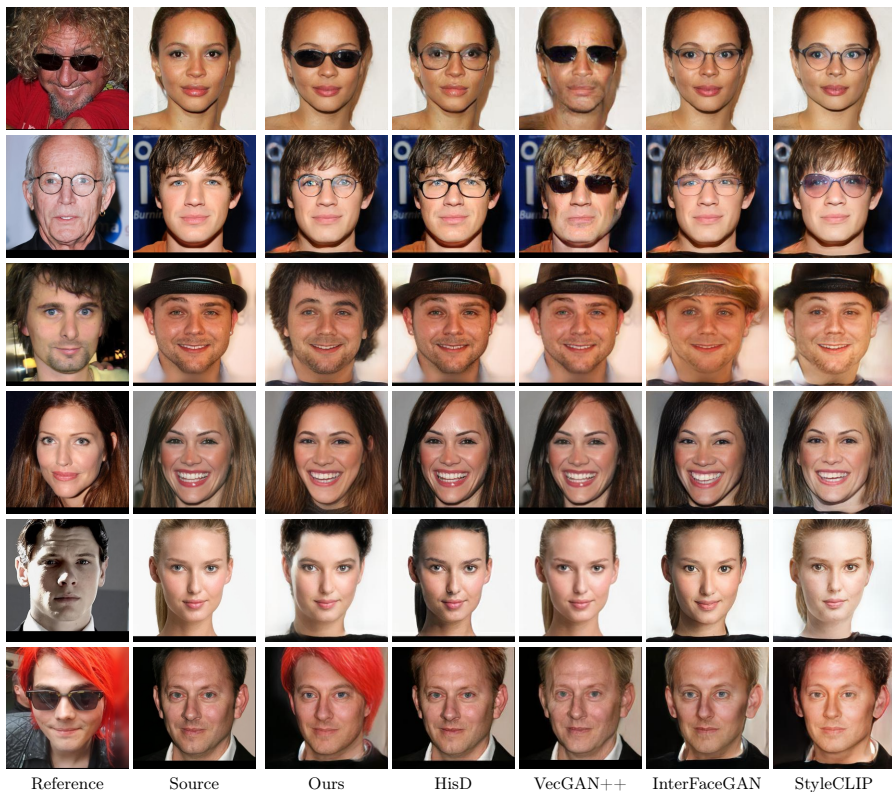


**Fig. 5:** Comparisons with the competing editing methods. Ours, HisD and VecGAN++ use the reference images when editing input images. For InterFaceGAN and StyleCLIP, we edit images by adding the corresponding directions for eyeglasses and changing hair colors. The first two examples show eyeglass addition edit and the others show hair editing.

**Table 2:** Results of our user study where participants are asked to identify the edited image. Based on this study, we find that our edits are challenging to distinguish.

	FFHQ				AFHQ		
	Eyes	Nose	Mouth	Overall	Eyes	Nose+Mouth	Overall
Original	40%	29%	34%	34%	40%	42%	41%
Ours (edited)	49%	59%	40%	49%	49%	43%	46%
Undecided	11%	13%	26%	16%	11%	15%	13%

By carrying over the hair from a reference image, our method is able to perform tasks like removing a person’s hat and changing their hairstyle, which is not achievable with other competing methods (5th row in Fig. 5). Notably, our approach can accommodate various hair colors, as demonstrated in the last row. Due to the rarity of these colors, HisD and VecGAN++ struggle to match the

**Table 3:** Quantitative ablation study of our editing. V1 is post-processing the triplane gradients, V2 is the implicit fusion, and V3 is fine-tuning the implicit fusion encoder.

V1	V2	V3	Eyeglasses			Hair		
			FID ↓	$\mathcal{M}_{SSIM}$ ↑	$\mathcal{M}_{\mathcal{L}_2}$ ↓	FID ↓	$\mathcal{M}_{SSIM}$ ↑	$\mathcal{M}_{\mathcal{L}_2}$ ↓
-	-	-	79.50	0.8451	0.0323	82.42	0.8177	0.0195
+	-	-	74.46	0.9814	0.0022	77.30	0.9674	0.0034
+	+	-	68.19	<b>0.9822</b>	<b>0.0020</b>	67.04	0.9691	0.0033
+	+	+	<b>66.68</b>	0.9818	0.0021	<b>64.59</b>	<b>0.9720</b>	<b>0.0029</b>

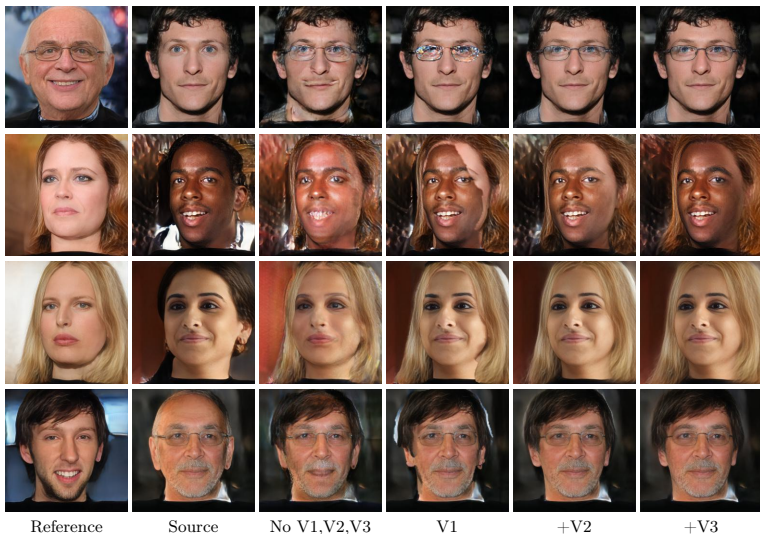


**Fig. 6:** Qualitative ablation study for glasses and hair edits, showing the effects of all fundamental stages of our pipeline.

same shade, while InterFaceGAN lacks a direction for red hair. Although we train a StyleCLIP direction for red hair, it also falls short in this regard.

Next, we present the outcomes of the user study we conducted among 25 participants. Given that comparable works are lacking for many of the reference-based edits we conduct, we present participants of our user study with both original and edited images and request them to identify the edited ones. We utilize the output of EG3D for both original and edited images to neutralize its influence on the results and provide the users with the same angle of the source and output images with random ordering. We also offer the option for participants to select "undecided" if they find it challenging to distinguish between the choices. This user study is conducted for mouth, eyes, and nose edits on the FFHQ dataset, and for eyes and nose+mouth edits on the AFHQ dataset as given in Tab. 2. We observe that some users select "undecided" for the majority

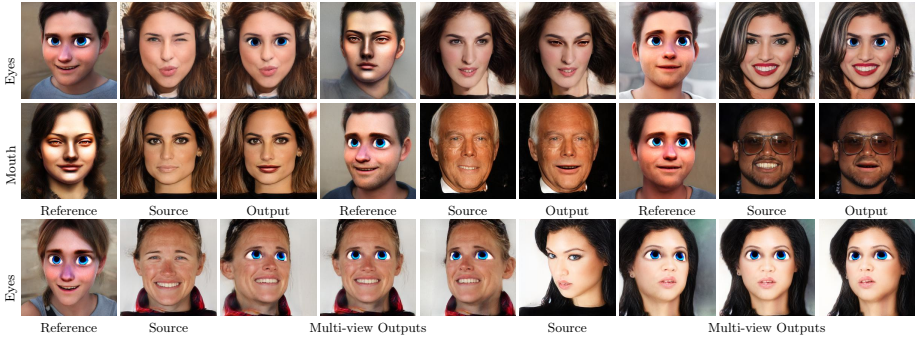


**Fig. 7:** Cross-generator edits with stylization. Our method achieves copying local parts from out-of-domain images such as from cartoon portraits.

of the choices. While some users do not use the "undecided" option, we find that their ability to correctly identify the edited image is close to random chance.

**Ablation study.** We demonstrate the improvements during the development of our pipeline stages step by step, both quantitatively and qualitatively, in Tab. 3 and Fig. 6, respectively. In our initial ablation experiment, we apply Eq. (1) to merge the triplanes using a mask calculated via autograd function without any post-processing. Due to the intricate volumetric function affecting many pixels for each value in the triplane, the mask generated before post-processing fails to provide clear stitching of images, resulting in blurry outputs. Following the introduction of post-processing (V1), as described in Sec. 3.1, we successfully achieve clear stitching, as depicted in Fig. 6. This allows us to transfer the hair of one person to our input while aligning the features using the canonical representation of the triplane. However, the resulting output still lacks realism because it combines features from two different images with varying illuminations, identities, and skin colors. To address the issue of smoothness at stitch boundaries, we follow Sec. 3.2 and perform encoding and decoding, via the pretrained encoder and decoder respectively, on the fused triplane. Since these encoders are trained with real images, they possess knowledge about real image priors. Despite the input image not being realistic, as shown in Fig. 6 (V1), the encoder successfully encodes its latent to EG3D’s natural latent space while attempting to preserve the identity (Fig. 6 (V2)). However, a pretrained encoder optimized for encoding real images to EG3D latent space may not be optimal for our specific use case. Consequently, we replace the encoder with one trained specifically for this task, as elaborated in Sec. 3.3. This specialized encoder ensures color preservation of the original identity and enhances editing details such as the coherence of eyeglass frames, and reducing background leakage (V3).

**Cross-generator edits.** We also provide novel edits, visualized in Fig. 7, where the reference and source triplanes are gathered from stylized and non-stylized generators, respectively. Specifically, we utilize [34] and fine-tune the EG3D backbones with different text prompts, such as: "3d human face, close up

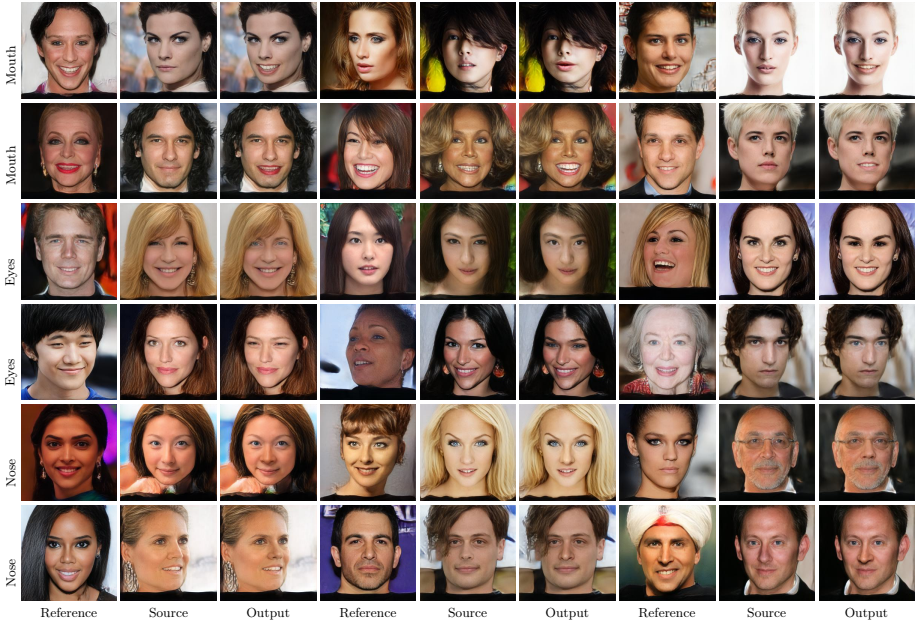


**Fig. 8:** Additional editing examples from the CelebA dataset, showcasing our method’s ability to seamlessly incorporate features such as lips, eyes, and nose from a reference image into our input.

cute and adorable, cute big circular reflective eyes, Pixar render, unreal engine cinematic smooth, intricate detail, cinematic". Then, we synthesize stylized triplanes and perform our reference-based editing on the triplanes of default EG3D. That is, we use the triplane from the fine-tuned generator as a reference one,  $\mathbf{T}_{\text{ref}}$ , and use the original EG3D for extracting the source triplane,  $\mathbf{T}_{\text{src}}$ . The rest of the steps are the same as before, using the original EG3D and encoder we train for EG3D. The results presented in Fig. 7 demonstrate our method’s independence from backbones, showcasing its capability to achieve part-based attribute stylization. This is different than previous approaches [34] that only offer global stylization.

**Additional Results.** We showcase more editing examples in Fig. 8, demonstrating challenging reference-based edits like transferring lips, eyeglasses, and nose from one person to another. We also show edits on the AFHQ dataset with our method in Fig. 9. This pipeline uses GOAE and EG3D, encoder and generator respectively, trained on the AFHQ dataset. Other than that it uses the same framework we use for CelebA face images. We also provide multi-view image results and more examples in Supplementary.

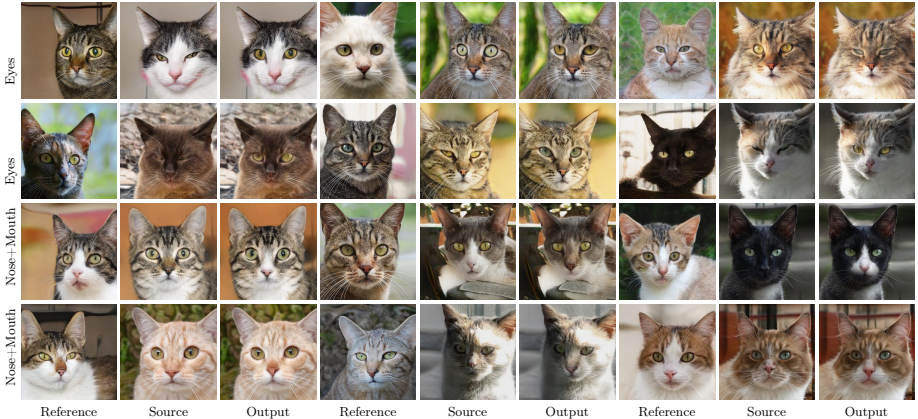


**Fig. 9:** Additional editing examples from AFHQ dataset. The nose and mouth are handled as a single part.

## 5 Conclusion

In conclusion, our work presents a comprehensive framework for reference-based, 3D-aware image editing, leveraging the unique capabilities of triplane latent spaces within the EG3D generator. Through spatial disentanglement and fusion learning, we achieve seamless integration of reference attributes while preserving the identity of the input image. Our approach fills a crucial gap in existing techniques by offering a unified solution that combines reference-based editing with 3D awareness, enabling versatile and high-fidelity image manipulations. Throughout our experiments, we have demonstrated the effectiveness and superiority of our framework over recent baseline methods in both quantitative and qualitative assessments.

In terms of limitations, our approach relies on the generation capabilities of EG3D, which, like StyleGAN, may struggle with background generation when trained on face portraits. Consequently, in some instances, rich background details may not be fully preserved. For instance, blurriness in the background can be observed in the fourth example of Fig. 5. However, this issue can be mitigated by masking out the background and avoiding reliance on EG3D for background generation.

## A Hyperparameters

We provide the mentioned hyperparameters of the main paper here.

**Triplane gradient post-processing.** We provide the code snippet in Listing 1 for post-processing stage, and the default parameters for  $\epsilon$ ,  $\mu$ , and  $\sigma$ . For the sake of simplicity, we omitted the batch dimension.

**Fusion of the triplanes.** Eq. (6) describes the fusion operation, where  $\mathbf{T}_{\text{imp}}$  is the implicitly fused triplane, and  $\mathcal{E}$  is the morphological erosion operation

```

1 import torchvision.transforms as T
2 def postprocess_tp_mask(t, smooth_tp=True,
3                       epsilon=(0.9, 1.1),
4                       mu=7, sigmas=(0.1, 2.0)):
5     blur_func = T.GaussianBlur(mu, sigma=sigmas)
6
7     t = t.view(-1,256,256) # 96 256 256
8     C,H,W = t.shape
9     for i in range(C):
10        t[i] -= torch.min(t[i])
11        t[i] /= torch.max(t[i])
12    for i in range(C):
13        mu = t[i].mean()
14        # take around mean region
15        t[i] = (t[i]<epsilon[1]*mu) * (t[i]>epsilon[0]*mu)
16        if smooth_tp:
17            t[i] = blur_func(t[i].unsqueeze(0)).squeeze(0)
18    # get the inverse, we are interested in outside of the mean
19    t = 1-t
20    # binarize
21    mean_grad = torch.mean(t, dim=0, keepdim=True).repeat(C,1,1)
22    b_mask = torch.zeros_like(mean_grad)
23    b_mask[mean_grad>mean_grad.mean()] = 1.0
24    if smooth_tp:
25        b_mask = blur_func(b_mask.unsqueeze(0)).squeeze(0)
26    t = b_mask
27    t = t.view(1,3,32,256,256)
28    return t

```

**Listing 1:** Post-processing the triplane gradients in Python.

applied on the post-processed triplane masks  $\mathbf{M}$ . Listing 2 describes the erosion operation with its default parameters.

$$\mathbf{T}_f = \mathcal{E}(\mathbf{M}_{\text{ref}}) * \mathbf{T}_{\text{ref}} + \mathcal{E}(\mathbf{M}_{\text{src}}) * \mathbf{T}_{\text{src}} + (\mathcal{E}(\mathbf{M}_{\text{src}}) - \mathcal{E}(\mathbf{M}_{\text{ref}})) * \mathbf{T}_{\text{imp}} \quad (6)$$

Morphological operations are realized with `max_pool2d` and Gaussian blurring. Note that `dilated_tp_mask` can be utilized when  $\mathbf{M}_{\text{ref}} = 1 - \mathbf{M}_{\text{src}}$  is set. Batch size is set to 1.

## B Additional visual results

We showcase additional reference-based editing results in Figs. 10 to 14 for glasses, hairstyle, mouth, nose, and eyes on CelebA, and Figs. 15 and 16 for eyes and nose on AFHQ dataset. Reference and input images are encoded and reconstructed via [42] for human portraits, and synthesised for animal faces.

```

1 import torch.nn.functional as F
2 import torchvision.transforms as T
3 def create_dilated_eroded_tp_masks(self, tp_mask,
4                                     blur_k_size=9, std_devs=(2.0,2.0),
5                                     morph_k_size=11):
6     blur = T.GaussianBlur(blur_k_size, sigma=std_devs)
7     dilated_tp_mask = blur(F.max_pool2d(tp_mask.view(1,96,256,256),
8                                         kernel_size=morph_k_size, stride=1,
9                                         padding=(morph_k_size - 1) // 2)).view(1,3,32,256,256)
10    eroded_tp_mask = blur((1 - F.max_pool2d((1 - tp_mask.view(1,96,256,256)),
11                                           kernel_size=morph_k_size, stride=1,
12                                           padding=(morph_k_size - 1) // 2))).view(1,3,32,256,256)
13    return eroded_tp_mask, dilated_tp_mask

```

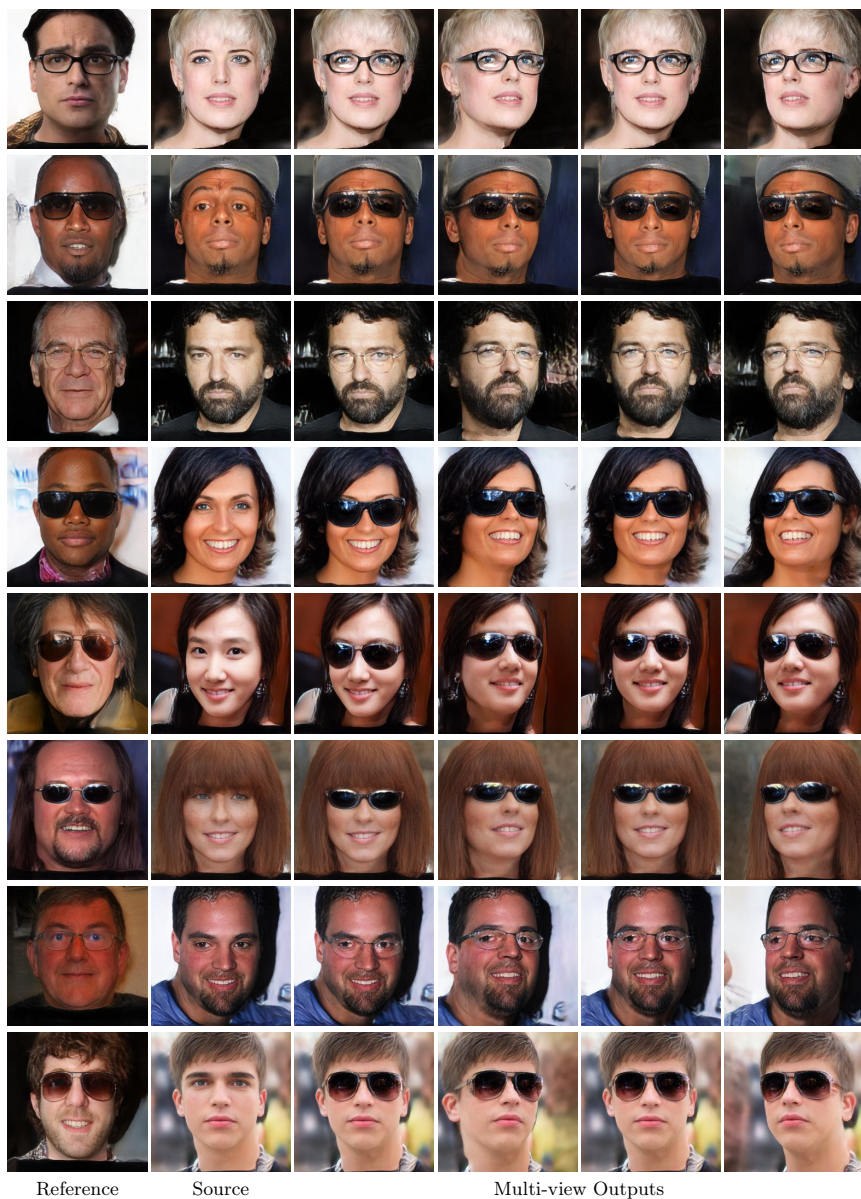
**Listing 2:** Dilating and eroding triplane masks in Python.

## C User study

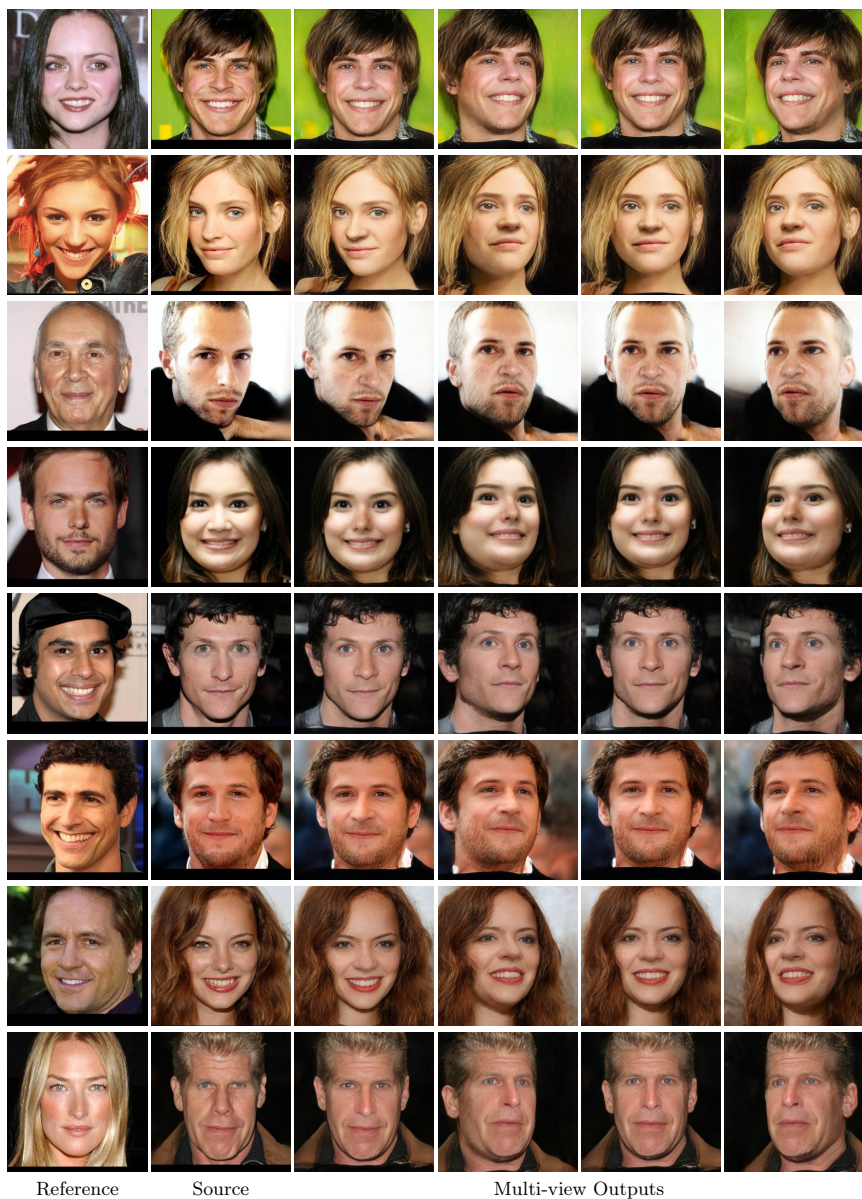
We provide additional samples for the top 3 incorrect and correct responses in Fig. 17. For the correct responses, even though the users were able to distinguish between edited and non-edited samples, the editing is still faithful to the source images as there are no visible artifacts.



Fig. 10: Hair edits and 3D visualizations.



**Fig. 11:** Glasses edits and 3D visualizations.



**Fig. 12:** Nose edits and 3D visualizations.

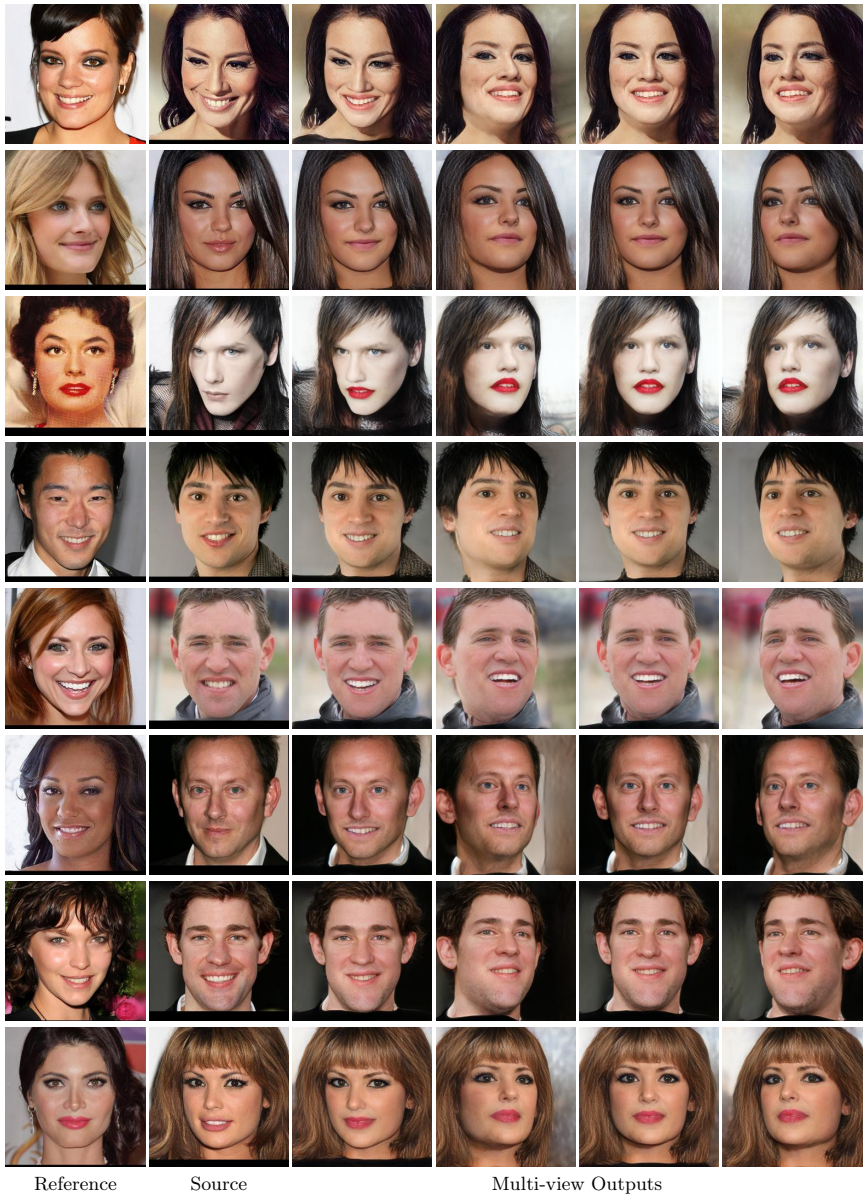


**Fig. 13:** Mouth edits and 3D visualizations.

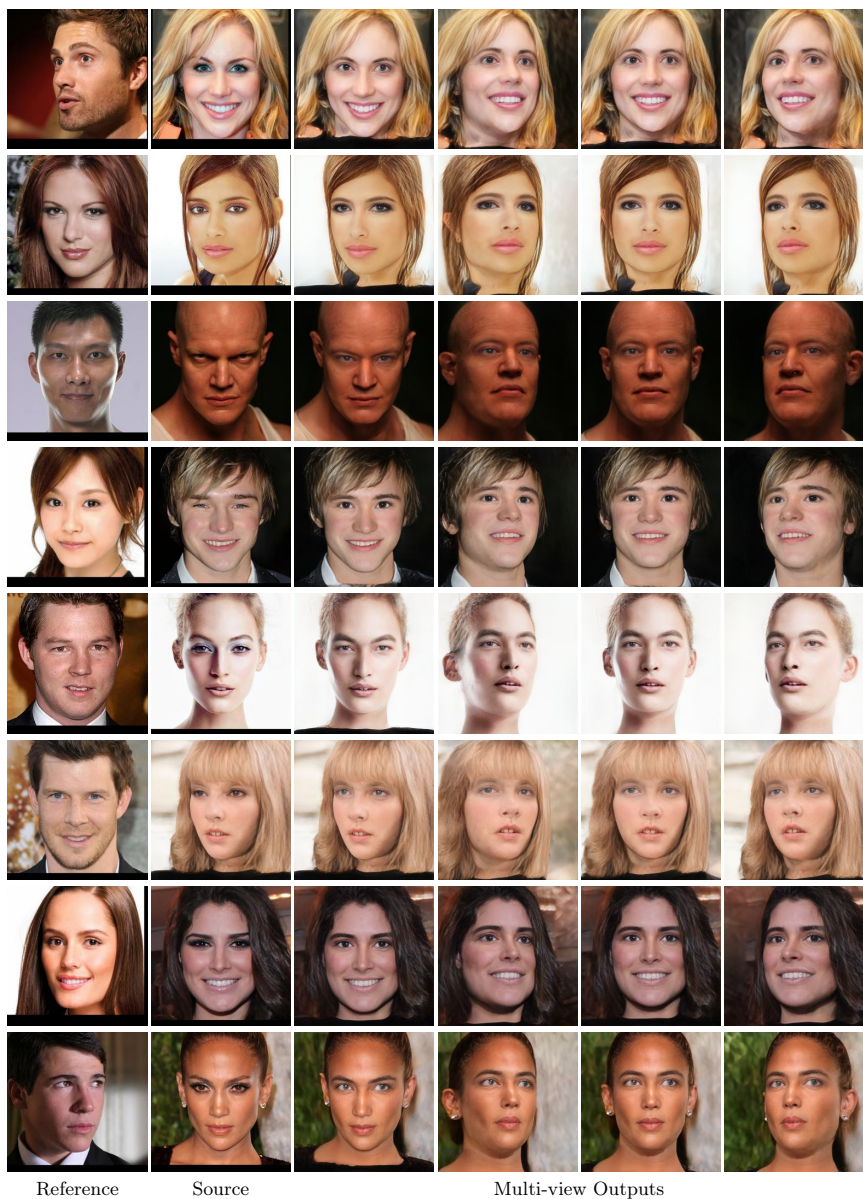


Fig. 14: Eyes edits and 3D visualizations.



**Fig. 15:** AFHQ eyes edits and 3D visualizations.



**Fig. 16:** AFHQ mouth & nose edits and 3D visualizations.

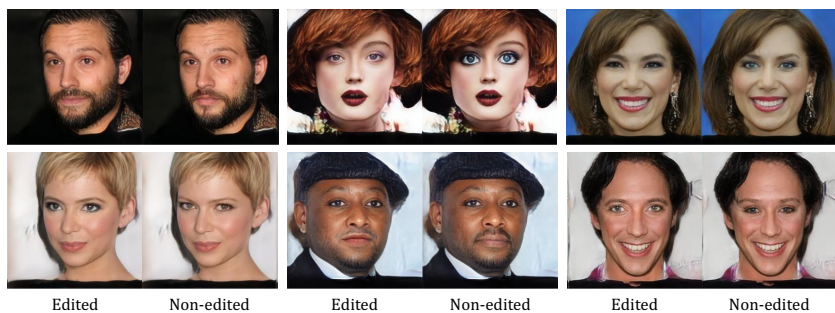


**Fig. 17:** Samples for top 3 most incorrect (first row) and correct (second row) responses on the user study. Incorrect responses correspond to the user not being able to distinguish between edited and non-edited samples, and vice versa for the correct responses.

## References

1. zllrunning. face-parsing.pytorch. <https://github.com/zllrunning/face-parsing.PyTorch/>, accessed: 2024-28-02
2. Abdal, R., Zhu, P., Mitra, N.J., Wonka, P.: Styleflow: Attribute-conditioned exploration of stylegan-generated images using conditional continuous normalizing flows. *ACM Transactions on Graphics (ToG)* **40**(3), 1–21 (2021)
3. Alaluf, Y., Patashnik, O., Cohen-Or, D.: Restyle: A residual-based stylegan encoder via iterative refinement. In: *Proceedings of the IEEE/CVF International Conference on Computer Vision*. pp. 6711–6720 (2021)
4. Bhattarai, A.R., Nießner, M., Sevastopolsky, A.: Triplanenet: An encoder for eg3d inversion (2024)
5. Chan, E.R., Lin, C.Z., Chan, M.A., Nagano, K., Pan, B., De Mello, S., Gallo, O., Guibas, L.J., Tremblay, J., Khamis, S., et al.: Efficient geometry-aware 3d generative adversarial networks. In: *Proceedings of the IEEE/CVF Conference on Computer Vision and Pattern Recognition*. pp. 16123–16133 (2022)
6. Chan, E.R., Monteiro, M., Kellnhofer, P., Wu, J., Wetzstein, G.: pi-gan: Periodic implicit generative adversarial networks for 3d-aware image synthesis. In: *Proceedings of the IEEE/CVF conference on computer vision and pattern recognition*. pp. 5799–5809 (2021)
7. Choi, Y., Uh, Y., Yoo, J., Ha, J.W.: Stargan v2: Diverse image synthesis for multiple domains. In: *Proceedings of the IEEE Conference on Computer Vision and Pattern Recognition* (2020)
8. Dalva, Y., Altindis, S.F., Dundar, A.: Vecgan: Image-to-image translation with interpretable latent directions. *Proceedings of the European conference on computer vision (ECCV)* (2022)
9. Dalva, Y., Pehlivan, H., Hatipoglu, O.I., Moran, C., Dundar, A.: Image-to-image translation with disentangled latent vectors for face editing. *IEEE Transactions on Pattern Analysis and Machine Intelligence* (2023)
10. Deng, J., Guo, J., Xue, N., Zafeiriou, S.: Arcface: Additive angular margin loss for deep face recognition. In: *Proceedings of the IEEE/CVF conference on computer vision and pattern recognition*. pp. 4690–4699 (2019)
11. Dundar, A., Saprà, K., Liu, G., Tao, A., Catanzaro, B.: Panoptic-based image synthesis. In: *Proceedings of the IEEE/CVF Conference on Computer Vision and Pattern Recognition*. pp. 8070–8079 (2020)
12. Goodfellow, I., Pouget-Abadie, J., Mirza, M., Xu, B., Warde-Farley, D., Ozair, S., Courville, A., Bengio, Y.: Generative adversarial nets. *Advances in neural information processing systems* **27** (2014)
13. Gu, J., Liu, L., Wang, P., Theobalt, C.: Stylenerf: A style-based 3d-aware generator for high-resolution image synthesis. *arXiv preprint arXiv:2110.08985* (2021)
14. Härkönen, E., Hertzmann, A., Lehtinen, J., Paris, S.: Ganspace: Discovering interpretable gan controls. *Advances in Neural Information Processing Systems* **33** (2020)
15. Heusel, M., Ramsauer, H., Unterthiner, T., Nessler, B., Hochreiter, S.: Gans trained by a two time-scale update rule converge to a local nash equilibrium. *Advances in neural information processing systems* **30** (2017)
16. Hou, X., Zhang, X., Liang, H., Shen, L., Lai, Z., Wan, J.: Guidedstyle: Attribute knowledge guided style manipulation for semantic face editing. *Neural Networks* **145**, 209–220 (2022)

17. Huang, X., Liu, M.Y., Belongie, S., Kautz, J.: Multimodal unsupervised image-to-image translation. *ECCV* (2018)
18. Karras, T., Laine, S., Aila, T.: A style-based generator architecture for generative adversarial networks. In: *Proceedings of the IEEE/CVF Conference on Computer Vision and Pattern Recognition*. pp. 4401–4410 (2019)
19. Karras, T., Laine, S., Aittala, M., Hellsten, J., Lehtinen, J., Aila, T.: Analyzing and improving the image quality of stylegan. In: *Proceedings of the IEEE/CVF Conference on Computer Vision and Pattern Recognition*. pp. 8110–8119 (2020)
20. Lei, B., Yu, K., Feng, M., Cui, M., Xie, X.: Diffusiongan3d: Boosting text-guided 3d generation and domain adaption by combining 3d gans and diffusion priors. *arXiv preprint arXiv:2312.16837* (2023)
21. Li, X., Zhang, S., Hu, J., Cao, L., Hong, X., Mao, X., Huang, F., Wu, Y., Ji, R.: Image-to-image translation via hierarchical style disentanglement. In: *Proceedings of the IEEE/CVF conference on computer vision and pattern recognition*. pp. 8639–8648 (2021)
22. Liu, G., Dundar, A., Shih, K.J., Wang, T.C., Reda, F.A., Sapra, K., Yu, Z., Yang, X., Tao, A., Catanzaro, B.: Partial convolution for padding, inpainting, and image synthesis. *IEEE Transactions on Pattern Analysis and Machine Intelligence* (2022)
23. Liu, L., Jiang, H., He, P., Chen, W., Liu, X., Gao, J., Han, J.: On the variance of the adaptive learning rate and beyond. In: *Proceedings of the Eighth International Conference on Learning Representations (ICLR 2020)* (April 2020)
24. Liu, Z., Luo, P., Wang, X., Tang, X.: Deep learning face attributes in the wild. In: *Proceedings of the IEEE international conference on computer vision*. pp. 3730–3738 (2015)
25. Lyu, Y., Chen, P., Sun, J., Peng, B., Wang, X., Dong, J.: Dran: detailed region-adaptive normalization for conditional image synthesis. *IEEE Transactions on Multimedia* (2023)
26. Lyu, Y., Dong, J., Peng, B., Wang, W., Tan, T.: Sogan: 3d-aware shadow and occlusion robust gan for makeup transfer. In: *Proceedings of the 29th ACM International conference on multimedia*. pp. 3601–3609 (2021)
27. Mildenhall, B., Srinivasan, P.P., Tancik, M., Barron, J.T., Ramamoorthi, R., Ng, R.: Nerf: Representing scenes as neural radiance fields for view synthesis. *Communications of the ACM* **65**(1), 99–106 (2021)
28. Or-El, R., Luo, X., Shan, M., Shechtman, E., Park, J.J., Kemelmacher-Shlizerman, I.: Stylesdf: High-resolution 3d-consistent image and geometry generation. In: *Proceedings of the IEEE/CVF Conference on Computer Vision and Pattern Recognition*. pp. 13503–13513 (2022)
29. Patashnik, O., Wu, Z., Shechtman, E., Cohen-Or, D., Lischinski, D.: Styleclip: Text-driven manipulation of stylegan imagery. In: *Proceedings of the IEEE/CVF International Conference on Computer Vision*. pp. 2085–2094 (2021)
30. Pehlivan, H., Dalva, Y., Dundar, A.: Styleres: Transforming the residuals for real image editing with stylegan. In: *Proceedings of the IEEE/CVF Conference on Computer Vision and Pattern Recognition*. pp. 1828–1837 (2023)
31. Richardson, E., Alaluf, Y., Patashnik, O., Nitzan, Y., Azar, Y., Shapiro, S., Cohen-Or, D.: Encoding in style: a stylegan encoder for image-to-image translation. In: *Proceedings of the IEEE/CVF conference on computer vision and pattern recognition*. pp. 2287–2296 (2021)
32. Shen, W., Liu, R.: Learning residual images for face attribute manipulation. In: *Proceedings of the IEEE conference on computer vision and pattern recognition*. pp. 4030–4038 (2017)

33. Shen, Y., Gu, J., Tang, X., Zhou, B.: Interpreting the latent space of gans for semantic face editing. In: Proceedings of the IEEE/CVF Conference on Computer Vision and Pattern Recognition. pp. 9243–9252 (2020)
34. Song, K., Han, L., Liu, B., Metaxas, D., Elgammal, A.: Diffusion guided domain adaptation of image generators. arXiv preprint <https://arxiv.org/abs/2212.04473> (2022)
35. Tov, O., Alaluf, Y., Nitzan, Y., Patashnik, O., Cohen-Or, D.: Designing an encoder for stylegan image manipulation. *ACM Transactions on Graphics (TOG)* **40**(4), 1–14 (2021)
36. Wu, Z., Lischinski, D., Shechtman, E.: Stylespace analysis: Disentangled controls for stylegan image generation. In: Proceedings of the IEEE/CVF Conference on Computer Vision and Pattern Recognition. pp. 12863–12872 (2021)
37. Xiao, T., Hong, J., Ma, J.: Elegant: Exchanging latent encodings with gan for transferring multiple face attributes. In: Proceedings of the European conference on computer vision (ECCV). pp. 168–184 (2018)
38. Xie, J., Ouyang, H., Piao, J., Lei, C., Chen, Q.: High-fidelity 3d gan inversion by pseudo-multi-view optimization. In: Proceedings of the IEEE/CVF Conference on Computer Vision and Pattern Recognition. pp. 321–331 (2023)
39. Yang, G., Fei, N., Ding, M., Liu, G., Lu, Z., Xiang, T.: L2m-gan: Learning to manipulate latent space semantics for facial attribute editing. In: Proceedings of the IEEE/CVF Conference on Computer Vision and Pattern Recognition. pp. 2951–2960 (2021)
40. Yildirim, A.B., Pehlivan, H., Bilecen, B.B., Dundar, A.: Diverse inpainting and editing with gan inversion. In: Proceedings of the IEEE/CVF International Conference on Computer Vision. pp. 23120–23130 (2023)
41. Yin, F., Zhang, Y., Wang, X., Wang, T., Li, X., Gong, Y., Fan, Y., Cun, X., Shan, Y., Oztireli, C., et al.: 3d gan inversion with facial symmetry prior. In: Proceedings of the IEEE/CVF Conference on Computer Vision and Pattern Recognition. pp. 342–351 (2023)
42. Yuan, Z., Zhu, Y., Li, Y., Liu, H., Yuan, C.: Make encoder great again in 3d gan inversion through geometry and occlusion-aware encoding. arXiv preprint [arXiv:2303.12326](https://arxiv.org/abs/2303.12326) (2023)
43. Zhang, G., Kan, M., Shan, S., Chen, X.: Generative adversarial network with spatial attention for face attribute editing. In: Proceedings of the European conference on computer vision (ECCV). pp. 417–432 (2018)
44. Zhang, M., Lucas, J., Ba, J., Hinton, G.E.: Lookahead optimizer: k steps forward, 1 step back. In: *Advances in Neural Information Processing Systems*. vol. 32. Curran Associates, Inc. (2019)
45. Zhang, R., Isola, P., Efros, A.A., Shechtman, E., Wang, O.: The unreasonable effectiveness of deep features as a perceptual metric. In: Proceedings of the IEEE Conference on Computer Vision and Pattern Recognition (CVPR) (June 2018)
46. Zhu, J.Y., Zhang, R., Pathak, D., Darrell, T., Efros, A.A., Wang, O., Shechtman, E.: Multimodal image-to-image translation by enforcing bi-cycle consistency. In: *Advances in neural information processing systems*. pp. 465–476 (2017)
47. Zhu, P., Abdal, R., Qin, Y., Wonka, P.: Sean: Image synthesis with semantic region-adaptive normalization. In: Proceedings of the IEEE/CVF Conference on Computer Vision and Pattern Recognition. pp. 5104–5113 (2020)